International Journal of Hydrogen Energy 88 (2024) 956–964

Contents lists available at ScienceDirect

International Journal of Hydrogen Energy

journal homepage: www.elsevier.com/locate/he

Unveiling the potential of ultra-low load Co on porous carbon-rich SiCN(O) fibre mats towards oxygen electrocatalysis in alkaline medium

Eranezhuth Wasan Awin [a], Marwan Ben Miled [b], Clément Comminges [c], Aurélien Habrioux [c], Samuel Bernard [b], Stefan Schafföner [a], Günter Motz [a,*]

[a] University of Bayreuth, Prof.-Rüdiger Bormann-Str. 1, 95447, Bayreuth, Germany
[b] Univ. Limoges, CNRS, IRCER, UMR 7315, F-87000, Limoges, France
[c] CNRS, IC2MP, UMR 7285, Univ. Poitiers, 4 Rue Michel Brunet, F86073, France

A B S T R A C T

The development of efficient and cost-effective catalysts for the oxygen electrocatalysis is crucial for advancing renewable energy technologies, such as fuel cells, electrolyzers and metal-air batteries. Herein, we report the high efficiency of Co nanoclusters generated on porous silicon oxycarbonitride (SiCN(O)) fibre mats towards Oxygen Reduction Reaction (ORR) and Oxygen Evolution Reaction (OER) in alkaline medium. Porous SiCN(O) ceramic fibrous supports were synthesized via electrospinning of a blend of oligosilazane Durazane 1800, polyacrylonitrile and polystyrene followed by an appropriate heat-treatment. Co nanoparticles with a remarkably low mass loading (4 wt%) were immobilized on the SiCN(O) fibres for efficient bifunctional catalytic activity towards OER/ORR. The catalysts exhibited ORR activity (onset potential (E_0) of 0.83 V *vs.* RHE) and excellent stability (80 h) in alkaline medium. Concomitantly, the catalyst required only 1.67 V to drive a current density of 10 mA cm^{-2} in 1 M KOH for OER.

1. Introduction

The societal and economic dependency on fossil fuels exacerbate the environmental issues. Hence, the transition from a petroleum-based economy to a CO_2 free energy grid requires the use of efficient and low-cost energy conversion and storage devices. Electrochemical systems such as electrolyzers, fuel cells and metal air batteries use electrochemical conversion reactions such as ORR and OER. ORR serves as the cathodic half-reaction in fuel cells and is a major factor that determines the efficiency of fuel cell. Conversely, OER functions as the anodic half-reaction in water electrolyzers. Metal-air batteries pose greater technological challenges due to their need for a recharging process. In these batteries, ORR takes place during discharge, while the reverse process (OER) occurs at the same electrode during charging. Undeniably, the state-of-the-art noble metals like Platinum or its alloys and IrO_2/RuO_2 are considered to be the heart of ORR/OER. However, these catalysts face a challenge due to resource exhaustion, impeding large scale application. Consequently, the search for alternative electrocatalysts has led to the exploration of noble metal-free catalysts, featuring transition metals (TMs = Fe, Co, and Ni) and nitrogen (N)-doped carbon materials, providing an efficient OER/ORR activity [1–4]. Notably, among these alternatives, Co-based catalysts have emerged as excellent OER/ORR electrocatalysts, witnessing significant improvements in recent years.

The overall OER/ORR activity depends predominantly on the available number of active sites and intrinsic activity of these sites. One promising approach to increase the number of active sites is to design one-dimensional (1D) porous supports. The porous nature of 1D support material facilitates pathways for mass diffusion and electron transfer and enhances the effective surface area. In addition to this, it helps to incorporate various functional species, thereby promoting the creation of more active sites [5]. The electrospinning technique produces fibrous mats with a consistently uniform diameter up on pyrolysis of green fibres. Impregnating nanostructured metal or metal oxide nanoparticles onto fibres results in catalysts with high functionality, thereby enhancing catalytic properties. This approach has been successfully used to develop cost effective heteroatom (N) doped carbonaceous 1D materials with Co anchored into it to form Co–N–C electrocatalysts [6,7].

Co–N–C electrocatalysts has gained immense interest owing to the excellent electrical conductivity (presence of carbon) and synergistic effects (between the host and active sites) [8,9]. Recently, Ki Ro Yoon et al. reported the bifunctional oxygen electrocatalysis of CoO_x@CoN_y nanorods on N-doped carbon nanofibre in alkaline media. The enhanced OER activity was attributed to the oxide layer formation on the nanorods whereas ORR activity was due to the synergistic effect of CoO_x@CoN_y and N-doped carbon nanofibre, leading to rapid charge transfer [7].

* Corresponding author.
E-mail address: Guenter.Motz@uni-bayreuth.de (G. Motz).

https://doi.org/10.1016/j.ijhydene.2024.09.206
Received 31 July 2024; Received in revised form 3 September 2024; Accepted 16 September 2024
Available online 24 September 2024

Previous reports suggest that at higher temperatures, Co could bind to pyridinic N-groups and form catalytically active Co-N_x [10]. In addition to this, the presence of N atoms on carbonaceous supports plays a crucial role towards promoting oxygen electrocatalysis since it modifies the electronic structure of carbon [8,9,11–14]. However, the use of carbonaceous materials as catalyst supports faces a technical challenge due to their limited resistance to corrosion [15]. Recently, silicon-based carbonaceous electrocatalysts showed reasonable ORR/OER activity in alkaline media [16,17]. The positive response towards ORR and OER activity was attributed to the modification of electronic band structure of carbon lattice by the incorporation of silicon and enhanced electron transfer rate, respectively. Nevertheless, doping of silicon disturbs the stability of carbon lattice due to the large atomic radius of silicon compared to carbon, thereby inducing strain. Hence, an alternative approach using organosilicon polymers as inorganic support precursors would be highly interesting.

The polymer derived ceramic (PDC) route uses preceramic polymers which contain elements such as silicon, carbon, nitrogen and/or oxygen in their backbone (i.e., organosilicon polymers) and allows ultimately producing highly porous, conductive, mechanically and chemically stable ceramics labelled PDC through shaping and appropriate heat-treatments [18,19]. The incorporation of TMs (in the form of TM complexes) into the polymers can impart enhanced PDC functionalities, such as catalytic activity [20,21], magnetic properties [22,23], and electronic conductivity [24,25]. Limited research has been reported on the electrocatalytic activity of 3d TMs on PDC based supports as potential electrocatalysts [26–33]. PDC offers a unique approach towards designing of stable supports for OER/ORR electrocatalysis in alkaline medium. Accordingly, the main aim of this work is to synthesize supported catalysts composed of a very low Co loaded and immobilized on porous carbon-rich SiCN(O) fibre mats derived from Co-modified preceramic polymers and explore their potential application towards OER/ORR occurring in alkaline medium. The phase evolution, structural and textural properties of the developed catalytic supports was evaluated using microscopy and diffraction/spectroscopic techniques. The bifunctional catalytic activity (ORR and OER) and stability of carbon-rich Co–SiCN(O) fibre mats in alkaline conditions were explored. As a result of its finely-tuned nanostructure, mesoporous carbon-rich Co–SiCN(O) fibre mats demonstrated an onset potential of 0.83 V for ORR, coupled with a low overpotential of 360 mV for OER (at a current density of 10 mA cm^{-2}), and exhibited sustained durability over the long term. The generalized procedure adopted for the preparation of ceramic fibres is depicted in Fig. 1.

2. Experimental details

2.1. Processing of porous carbon rich SiCN(O) ceramic fibrous supports

A blend of oligosilazane Durazane 1800 (D1800, Merck (Germany)), polyacrylonitrile (PAN, Dolan GmbH (Germany)) and polystyrene (PS, Sigma-Aldrich (Germany)) were used as the precursors for processing carbon rich SiCN fibres. Polystyrene was used as the sacrificial compound and all the experiments were carried out in an inert atmosphere. In a typical experiment, 1 g of PAN was mixed with 0.7 g of PS and 0.25 g of D1800 were mixed together using dimethylformamide (DMF) as a solvent until a homogenous solution is obtained. The prepared solution was loaded in to 1 ml syringe and was subjected to electrospinning. A positive voltage of 9 kV was applied to the needle and a negative voltage of −8 kV was applied to the collector. The distance of the needle to collector was set to 10 cm. The flow rate was maintained to be 1 mL h^{-1}. The green fibres were stabilized under air at 250 °C for 1 h maintaining a heating rate 1 °C/min. The fibres were subsequently pyrolyzed under nitrogen atmosphere according to the following heating program resulting in the formation of amorphous SiCN support.

$$RT \xrightarrow{5^0c\ min^{-1}} 200^0c \xrightarrow{1^0c\ min^{-1}} 400^0c \xrightarrow{5^0c\ min^{-1}} 1000^0c(1h)$$

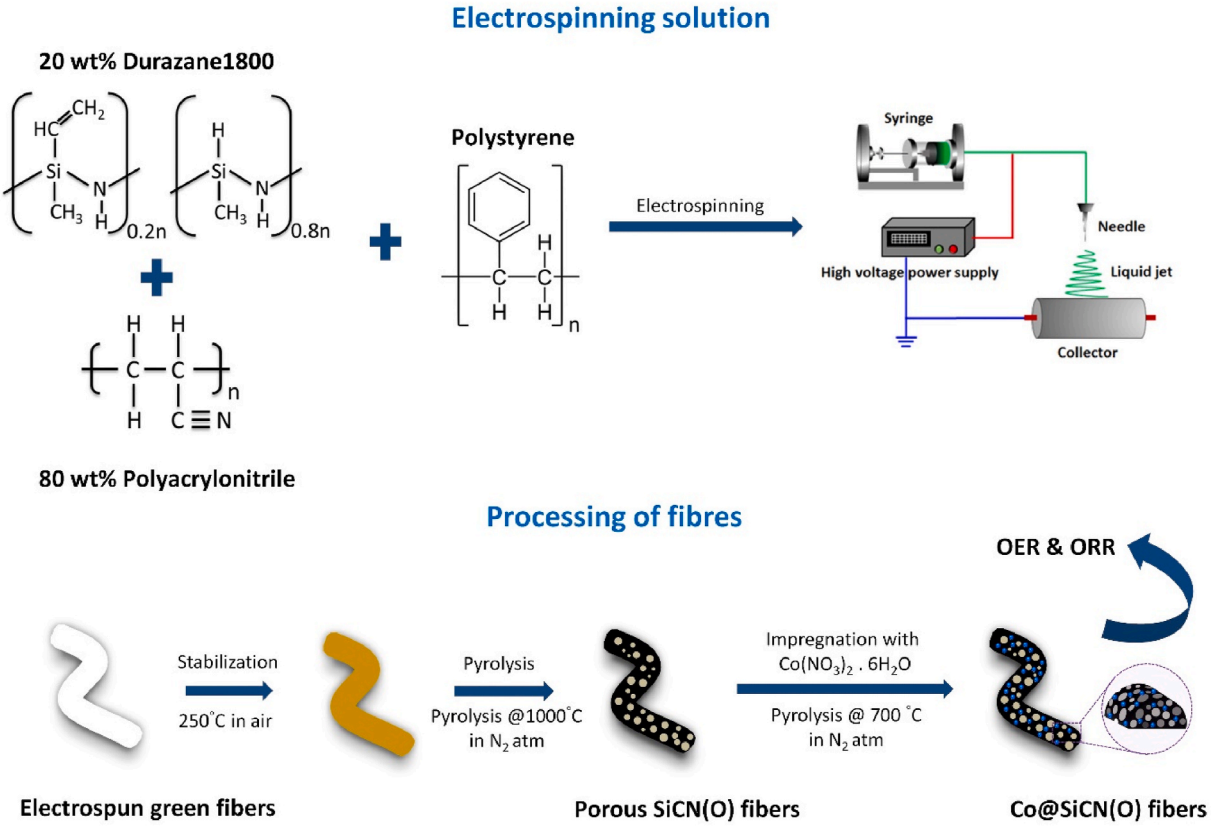

Fig. 1. Generalized scheme for the preparation of catalytic fibres.

2.2. Impregnation of Co catalyst in to C–SiCN(O) fibrous supports

The support material (500 mg) was then to added to an aqueous solution (10 mL H_2O) of 102.9 mg $Co(NO_3)_2 \times 6H_2O$ and stirred at 110 °C for 2 h to impregnate Co into the porous substrate. The solvent was removed and the coated material pyrolyzed under nitrogen atmosphere according to the following heating program:

$$RT \xrightarrow{2^0c\ min^{-1}} 300^0c \xrightarrow{5^0c\ min^{-1}} 700^0c(0.5h)$$

2.3. Characterization

The thermogravimetric analysis (TGA) was done using a Netzsch STA 449 F3 Jupiter equipment (Netzsch GmbH, Germany) to determine the mass loss behaviour of the composites. The mass loss behaviour was determined in two steps. Initially, the green fibres were heated from 25 °C to 250 °C maintaining a heating rate of 5 K/min in ambient conditions to replicate the stabilization process. Subsequently, the fibres were heated to 1000 °C at 5 °C/min in nitrogen atmosphere. Prior to the measurements, the green fibres were dried in vacuum at 75 °C for 48 h to eliminate the presence of solvents. The pyrolyzed samples were crushed and the phase evolution was investigated using an X-ray diffractometer (Bruker AXS, Germany) using monochromatic CuKα radiation. The presence of free carbon was determined using Raman spectroscopy measurements (Bruker SENTERRA II, USA confocal microscope) with a 532 nm excitation laser. X-ray photoelectron spectroscopy (XPS) studies were carried out using an AlKα source (1486.6 eV) and a PHI 5000 VersaProbe III spectrometer. Monochromatic X-rays were produced using quartz crystal. The samples were placed on double sided sticky Kapton tape. The structural characterization of the prepared ceramic nanocomposites was performed using Scanning electron microscope (SEM, Gemini Sigma 300 VP, Carl Zeiss AG, Germany) and Transmission electron microscope (TEM, JEOL JEM 2200FS, 200 kV, Germany).

The electrocatalytic measurements were performed using a three-electrode home-made Teflon cell. Experiments were carried out in a 1 M KOH electrolyte (Sigma-Aldrich, 90%). A glassy carbon disk (geometric surface of 0.196 cm^2) served as the working electrode, while a glassy carbon electrode and a commercial reference hydrogen electrode (RHE – Gaskatel)) were used as the counter and reference electrodes, respectively. The catalyst ink was prepared by dispersing 10 mg of the catalyst in a solution composed of 250 μL of isopropanol and 750 μL of ultrapure water (UP). The resulting mixture was supplemented with 60 μL of Nafion® (5 wt% in a mixture of aliphatic alcohols, Sigma-Aldric) and subsequently sonicated for 30 min to ensure a homogeneous dispersion. For each experiment, 5 μL of the prepared ink was carefully deposited onto the glassy carbon disc. The drop was then allowed to dry for a few minutes a-under nitrogen atmosphere. The catalyst loading was thus 0.24 mg cm^{-2}, and the Co loading was found to be 0.01 mg cm^{-2}. Prior to OER and ORR measurements, cyclic voltammograms were recorded to stabilize the electrode/electrolyte interface. OER and ORR polarization curves were recorded at 5 mV s^{-1}. OER polarization curves were IR-corrected by calculating the ohmic drop thanks to impedance spectroscopy measurements carried out in a faradaic region in between 100 kHz and 10 Hz with an amplitude of 10 mV. To explore the effect of metal loading on OER, the Co loading was increased to 0.1 mg cm^{-2} and compared to the original loading. In order to test the durability of the prepared catalysts, chronopotentiometric measurements were performed for 80 h. The stability experiment was conducted using a homemade Teflon working electrode, designed to allow a continuous flow of oxygen for performing ORR. However, even with the slowest possible flow rate, some oxygen bubbles tend to accumulate on the surface and were difficult to remove. These bubbles were responsible for limiting the contact between the electrode and the electrolyte. Thus, the electrode potential increases dramatically, eventually reaching the detection limits of the potentiostat and creating a spike. This spike only disappears when the bubble is removed. To mitigate this issue, a rotating magnet was installed inside the cell, which helped to reduce the frequency of these spikes. Bubble removal remains a persistent challenge in this type of experiment. The spikes were removed in the stability result while plotting.

3. Results and discussion

The stabilization process typically involves heating PAN fibres in air or an oxidative environment at temperatures ranging from 250 °C to 320 °C. The main reactions that occurs during the stabilization process are cyclization of nitrile groups, oxidation of PAN (resulting in the formation of cross-links between polymer chains) and dehydrogenation. The PAN fibres are converted into a stable, infusible, and thermoset structure that can withstand the high temperatures of carbonization after stabilization [34]. In this work, the stabilization process was carried out at 250 °C in air and showed negligible mass loss as shown in Fig. 2a. TGA analysis (Fig. 2b) clearly revealed that PS degrades completely at ~400 °C. In the case of PAN, stabilization process typically occurs at temperatures between ~250 and 320 °C and the mass loss occurring at temperatures in the range of 270–500 °C could be attributed to the degradation of PAN backbone with the release of volatile gases such as hydrogen cyanide and ammonia. The mass loss at higher temperatures (above 700 °C) could be attributed to the carbonization of PAN [34]. Meanwhile, Durazane 1800 decomposes through a three-step process. The first step involves the degradation of volatile oligomers. The second step, occurring between 290 °C and 550 °C, includes dehydrogenation and transamination reactions. The third step (550 °C and 820 °C) is due to the polymer-to-ceramic transformation. The mass loss of pure Durazane 1800 was found to be ~23 %. The multiple mass loss observed for Durazane 1800-PAN-PS could be attributed to the combination of the degradation of PS (~300–400 °C), carbonization of PAN and ceramization of Durazane 1800 at higher temperatures. The stabilization, carbonization and ceramization process of the produced green fibres (Durazane 1800-PAN-PS) resulted in a yield of 52 %.

The polymeric blend solution exhibited a shear-thinning behaviour, Fig. 3 and this resulted in a seamless, bead and droplet free fibres (inset of Fig. 3) with an average fibre diameter of 500 nm. The high shear rates resulted in the reduction of viscosity of the polymeric blend solution due to the polymer chain disentanglement and alignment.

The colour of as-spun fibres changed from white to brown after the stabilization process implying that the oxidation of as-spun fibres at 250 °C and subsequent crosslinking/cyclization of PAN as well as possible crosslinking of Durazane 1800. After the stabilization process, the fibres were pyrolyzed at 1000 °C in N_2 atmosphere resulting in carbon-rich SiCN(O) fibres (black colour) with mesoporous nature. The fibre diameter reduced to 350 nm and the average pore size (analysed using ImageJ software) from SEM was found be less than 50 nm after pyrolysis. The carbon rich porous support and Co modified fibres will be hereafter referred as SiCN(O) and Co–SiCN(O)_700 respectively.

XRD analysis were performed on SiCN(O) and Co–SiCN(O)_700 over a 2θ range of 10–90° to investigate their crystallographic properties (Fig. 4a). The support and the catalysts were found to be amorphous in nature. The broad reflection observed at $2\theta = 12^\circ$ for SiCN(O) could be attributed to the presence of an amorphous phase. The observed broad peak at ~22° and 44° for Co–SiCN(O)_700 is an indication for the presence of amorphous carbon [35]. In addition to this, the peak at ~44° could also be assigned to the (111) planes of Co (ICDD 00-015-0806). The observance of negatively shifted carbon peak in the XRD data suggests lattice expansion and an increased presence of defects in the material. The Raman spectra of the samples revealed distinct D and G bands at 1333 cm^{-1} and 1581 cm^{-1}, respectively, confirming the existence of free carbon (Fig. 4b). The characteristic D bands indicate the presence of defects or disorder in the carbon structure and the G bands represents ordered carbon regions in the samples. The D and G peaks were accompanied by three peaks, peaks centered at ca. 1200 cm^{-1} (T) and

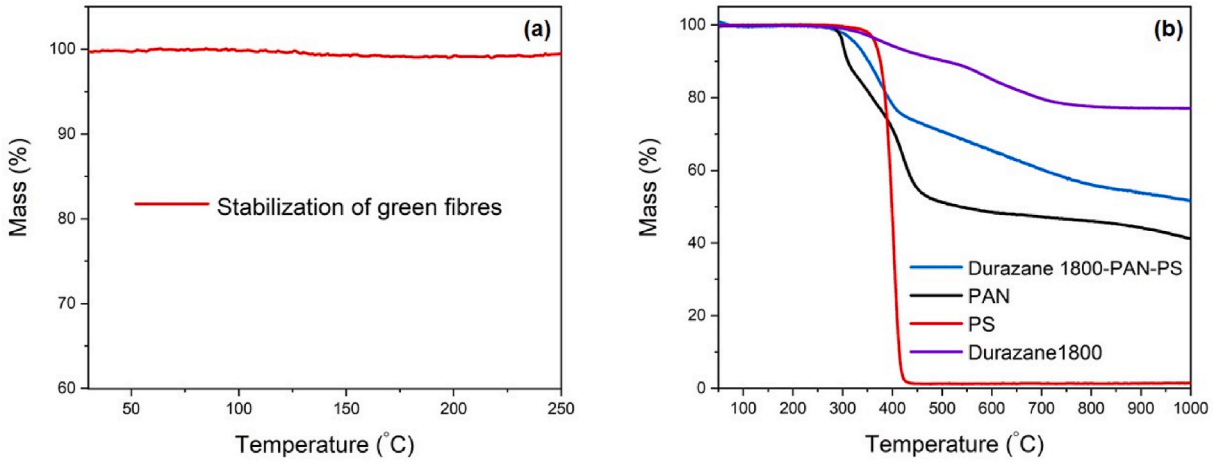

Fig. 2. Mass loss behaviour during the (a) stabilization of green fibres and (b) pyrolysis of Durazane 1800-PAN-PS (electrospun fibres), Durazane 1800, PAN and PS. (For interpretation of the references to colour in this figure legend, the reader is referred to the Web version of this article.)

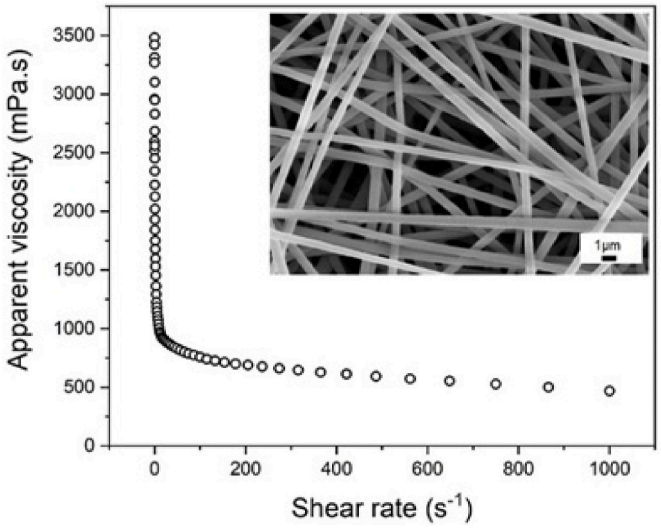

Fig. 3. Dependency of viscosity on shear rate of polymer blend solution exhibiting a shear thinning behaviour. Inset images depicts SEM of electrospun green fibres.

1500 cm^{-1} (D″) ascribed to amorphous carbon, and another mode centered at ca. 1610 cm^{-1} (often called G' mode) is associated with disorder induced double resonance process. The disordered state of the material, as indicated by the T and D" bands could have arised from several factors such as the existence of pores, presence of edges in the graphene layers, deviations from the planarity of these layers and the presence of sp^3 carbon atoms [36]. The I_D/I_G ratio determines the degree of graphitization, the amount of defects, and the in-plane crystallite size (La) in graphene materials. In this study, it was found that the addition of cobalt had no significant influence on the I_D/I_G ratio. The La was calculated to be approximately 14 nm using the following relation.

$$La\ (nm) = (2.4 \times 10^{-10})\ \lambda_L^4\ I_G/I_D \quad (1)$$

where λ_L is the wavelength of laser in nm.

The existence of Co was confirmed by Inductively coupled plasma optical emission spectrometry (ICP-OES) and indicated 3.67 wt% Co in the material. The absence of Co signals in XRD could be correlated to the presence of only a small amount of Co nanocrystals content in the catalyst.

The SEM of SiCN(O) and Co–SiCN(O)_700 revealed three-dimensional network structures consisting of interlaced nanofibres, Fig. 5a and b respectively. Post-pyrolysis SEM analysis depicts retention of interconnected structure, resulting in a material with high interrelated porosity and internal channels. The modification of carbon rich SiCN(O) fibres with Co did not have profound influence on the morphology of the fibres as seen in Fig. 5b. The inset image of Fig. 5a and b clearly revealed mesoporous channels in the pyrolyzed fibres.

The investigation of the prepared fibres using HR-TEM revealed continuous nanochannels (in the range of 25–30 nm) with uniform distribution of Co nanocrystals in porous SiCN(O) fibres as shown in Fig. 6a. The Co nanocrystals was found to have an average size of 8 nm (Fig. 6b). The Co nanocrystals within the SiCN(O) support had a lattice fringe spacing of 0.2 nm, assigned to the (111) plane (inset of Fig. 6c) of metallic Co. The presence of a SiCN(O) matrix serves to inhibit the agglomeration of Co nanocrystals. Even though most of Co nanocrystals were uniformly distributed across the fibres, the analysis of HR-TEM provided additional insight, revealing that some of the metallic Co particles were encapsulated by nitrogen doped turbostratic carbon, signifying a specific carbon arrangement around the Co nanocrystals (Fig. 6c). Since Co–SiCN(O)_700 catalysts were prepared using a precursor route, the observed carbon shell could also have been doped with nitrogen. In this case, the Co nanocrystals were not directly exposed to the electrolyte. However, the synergetic interaction between Co and nitrogen doped carbon is expected to induce ORR activity. The embedment of Co nanocrystals by the nitrogen doped carbon layer is also believed to enhance the stability of the catalyst under harsh operating conditions. The TEM analysis of Co–SiCN_500 revealed smaller Co crystallites and increasing the temperature (Co–SiCN_900) resulted in the formation of large sized crystallites as exemplified in Figs. S2(a) and (b).

Fig. 7 illustrates the XPS measurements to assess surface composition and chemical states of the Co–SiCN(O) catalysts. The obtained XPS survey data affirmed the presence of Si, C, N, O, and Co on the surface of the catalysts. XPS analysis of Co 2p spectra revealed that metallic Co and Co oxides were located at the surface of the fibres (Fig. 7a). The analysis of the Co $2p_{3/2}$ peaks shows a prominent peak at 776.1 eV, which corresponds to metallic Co. Additionally, another significant peak was observed at 779.6 eV, indicating the presence of Co oxides. Furthermore, a satellite peak was detected at 783.7 eV, further confirming the characteristics of the cobalt species present in the sample. Besides Co functioning as an active site, the high-resolution N 1s spectra (Fig. 7b) highlighted distinctive peaks of different binding modes of nitrogen. The deconvolution resulted in the observance of pyridinic-N (398.2 eV), pyrrolic-N (399.1 eV), graphitic-N (400.9 eV) and N-oxide (402.6 eV) modes of nitrogen. The pyridinic N-edge plane heteroatom is

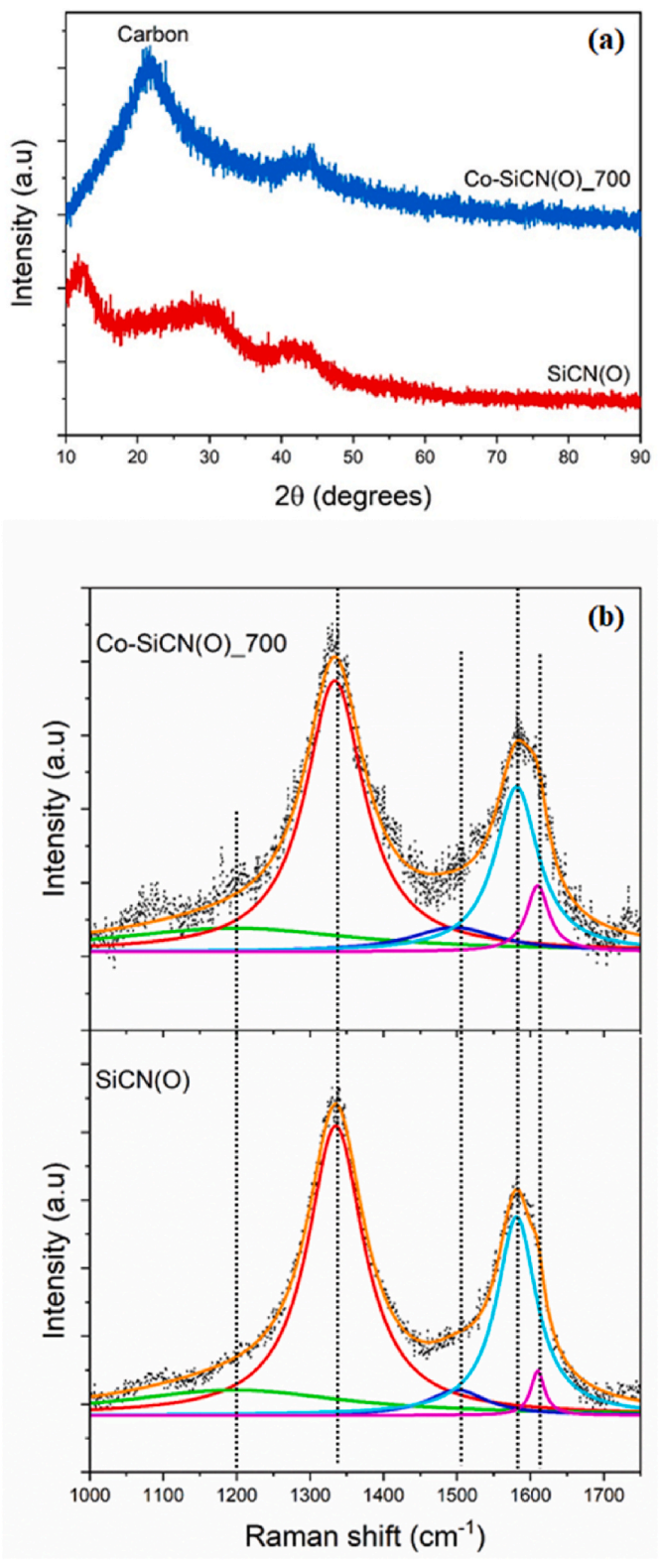

Fig. 4. (A) XRD and (b) Raman spectra of catalysts, revealing the amorphous nature and presence of free carbon respectively.

characterized by its presence in a sp^2 carbon framework, where it is bonded to two carbon atoms at the edge whereas the pyrrolic-N bond involves a nitrogen atom bonded to a five-membered sp^2 carbon ring. In graphitic-N, the nitrogen atom is a part of the in-plane heteroatom arrangement within the carbon framework. The presence of these nitrogen functionalities alters the electronic structure, making the material more conducive to catalyzing ORR. In particular, pyridinic N, with its lone electron pair situated in the plane of the carbon matrix, plays a crucial role in promoting ORR [37]. Furthermore, graphitic-N is associated with high electrical conductivity, further enhancing the overall catalytic performance. The deconvolution of C1s spectra (Fig. 7c) revealed the presence of C–C, C–N, C═O and π-π* peaks at 284.6 eV, 286.5 eV, 288.8 eV and 290.8 eV respectively [38]. The π-π* satellite peak (delocalized π electrons) indicates the presence of electrically conductive sp^2 carbon [39]. These findings provide substantial evidence for overall enhancement of catalytic activity due to high electrical conductivity.

The N1s spectra of SiCN(O) revealed the presence of pyridinic-N, pyrrolic-N and graphitic-N modes of nitrogen, Fig. S3(a). The binding energies the aforementioned modes of nitrogen did not change even after the Co addition. Hence, there is no substantial evidence to prove the formation of Co-N_x bonds from the XPS analysis. The C1s spectra showed no significant change for both SiCN(O) and Co–SiCN(O) samples as shown in Fig. S3(b).

3.1. Electrocatalytic activity

The electrocatalytic properties of Co–SiCN(O)_700 fibres were investigated under rotating disk electrode (RDE) an O_2 saturated 1 M KOH solution at 1600 rpm. The Co–SiCN(O)_700 fibres exhibited a noticeable impact on the ORR activity in comparison to its unmodified SiCN(O) counterpart as shown in Fig. 8a showing that Co nanoparticles are the ORR active entities. The onset potential for oxygen reduction reaction (ORR) was determined to be 0.83 V *vs.* RHE and the half-wave potential was ca. 0.78 V vs. RHE. Upon increasing the rotation rates, a significant rise in current density was observed (Fig. S4(a)), suggesting enhanced mass transport of oxygen. The Koutecký-Levich (K-L) plot (Fig. S4(b)) for ORR exhibited a clear 2-electron pathway and the active sites/mechanism of the ORR were found to be closely associated to the structural/spectroscopic characteristics of the catalyst. The spectroscopic analysis revealed Co/CoO as active sites, playing a significant role in the ORR mechanism. Co nanocrystals exhibits multiple oxidation states such as +2, +2/+3 and + 3 depending on the pH and potential of the environments. In high potential regions with in alkaline environments the Co species are closely associated with the reduction potential from Co_3O_4 to CoO as given by equation (2).

$$Co_3O_4 + H_2O + 2e^- \rightarrow 3CoO + 2OH^- \quad (2)$$

This suggests that CoO/$Co(OH)_2$ probably serve as the active sites for oxygen reduction in such alkaline conditions. In alkaline conditions, the surface is likely covered by $Co(OH)_2$. In this context, initially $Co(OH)_2$ reacts with oxygen, forming a bound superoxide. Then, the bound superoxide receives a proton, converting it into a bound peroxide. This is followed by the reduction of Co(III) sites, thereby releasing peroxide anions. Subsequent reduction of Co(III) and proton extraction from water results in the regeneration of Co surface [40]. In addition to this, the enhancement in ORR activity could also be attributed to the synergistic interaction between Co/CoO and nitrogen doped carbon as revealed by Fig. 6c. It is assumed that the encapsulated Co nanocrystals activates the nitrogen doped carbon layers, providing the outer surface to participate in the ORR [41,42].

The effect of pyrolysis temperature on ORR activity was also investigated and is shown in Fig. 8b. The linear sweep voltammetry (LSV) curve for Co–SiCN_700 revealed the highest limiting current density compared to all other samples, probably indicating a better accessibility of active sites of oxygen. Interestingly, the support material (SiCN(O)) was also found to exhibit ORR activity. Indeed, SiCN(O) could be regarded as a co-catalyst and the presence of Co provides additional active sites. The XRD analysis of the Co–SiCN(O)_500 sample revealed that the material is predominantly amorphous (Fig. S1). In contrast, Co–SiCN(O)_900 sample displayed a peak at around $2\theta = 25.8^{\circ}$, which

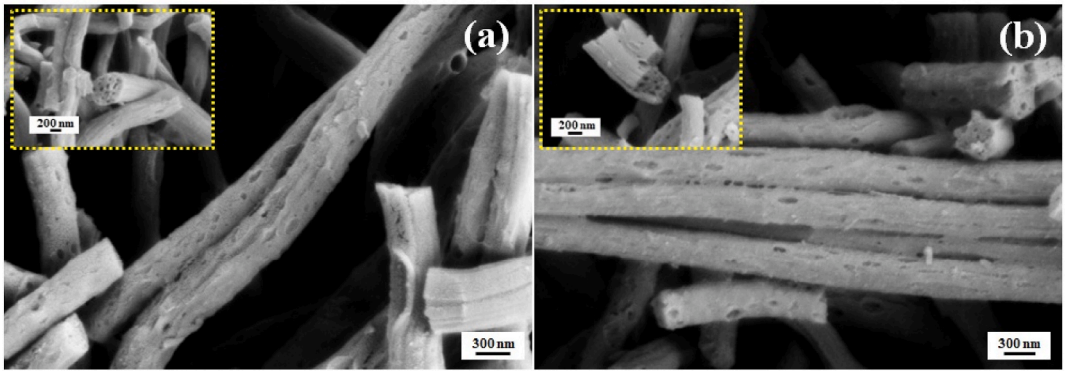

Fig. 5. SEM of (a) SiCN(O) and (b) Co–SiCN(O)_700 revealing the porous nature of pyrolyzed fibres.

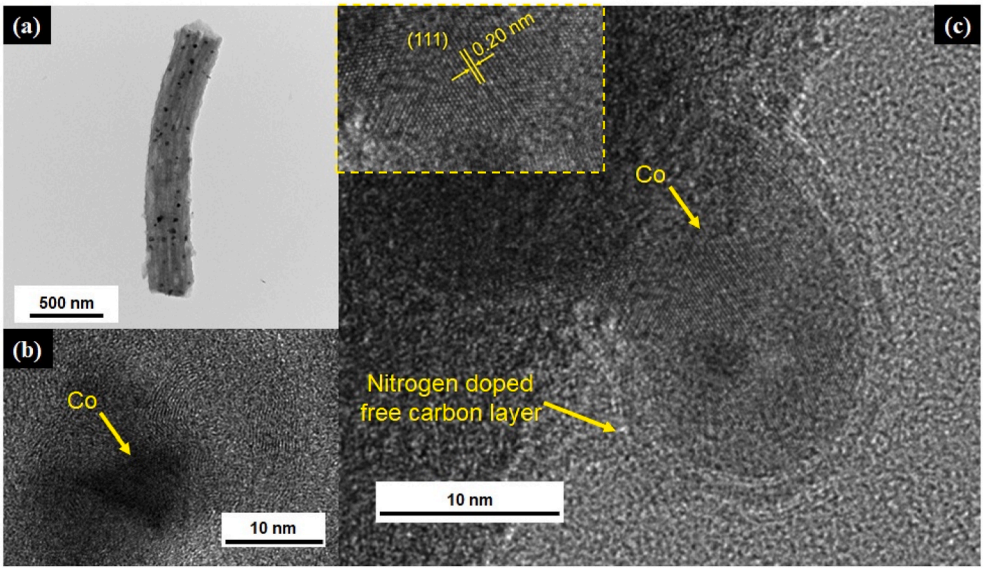

Fig. 6. TEM of **(a, b)** Co–SiCN(O)_700 exhibiting uniform distribution of Co nanocrystals in SiCN(O) matrix and **(c)** HR-TEM of Co–SiCN(O)_700 showcasing embedment of Co in a nitrogen doped turbostratic free carbon.

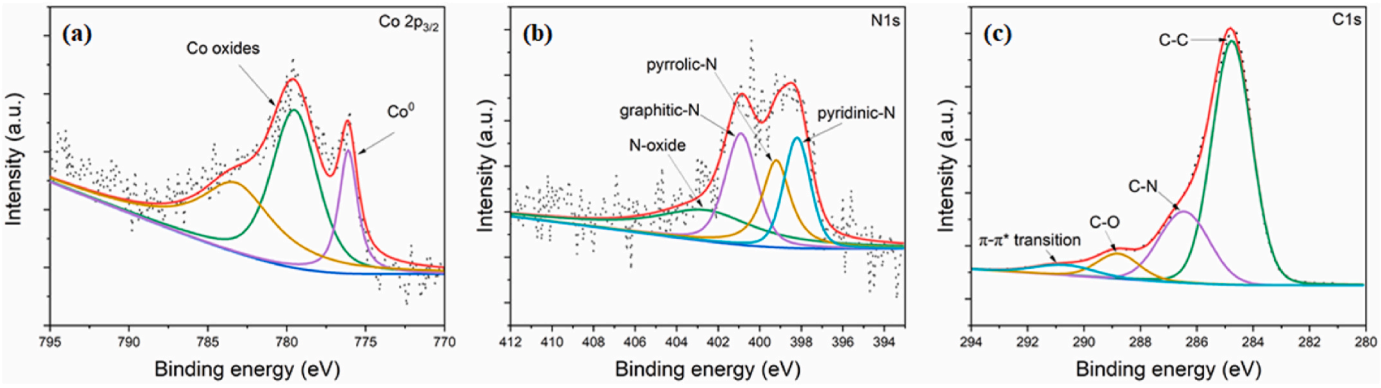

Fig. 7. High resolution XPS spectra of (a) Co2p confirming the presence of metallic Co and Co oxide species (b) N1s verifying the existence of different binding modes of nitrogen and (c) C1s revealing the π-π* satellite peak.

corresponds to the (002) diffraction of the graphitic layer-by-layer structure. Furthermore, the Co–SiCN(O)_900 sample exhibited a sharpened peak at around $2\theta = 44^{\circ}$, indicating the presence of larger Co crystals. In the case of Co–SiCN_900, TEM revealed that an increase in pyrolysis temperatures could lead to the aggregation of Co nanocrystals resulting in the formation larger particles (Fig. S2) corroborating the XRD analysis. This structural evolution could be correlated to a decrease in the number of active sites for ORR. Additionally, the increase in pyrolysis temperature could also be associated to reduced nitrogen content in the catalysts [43,44]. Chronopotentiometric measurements were carried out at 10 mA cm^{-2} in order to understand the stability of the prepared catalyst. The catalysts were found to be stable even after 80 h

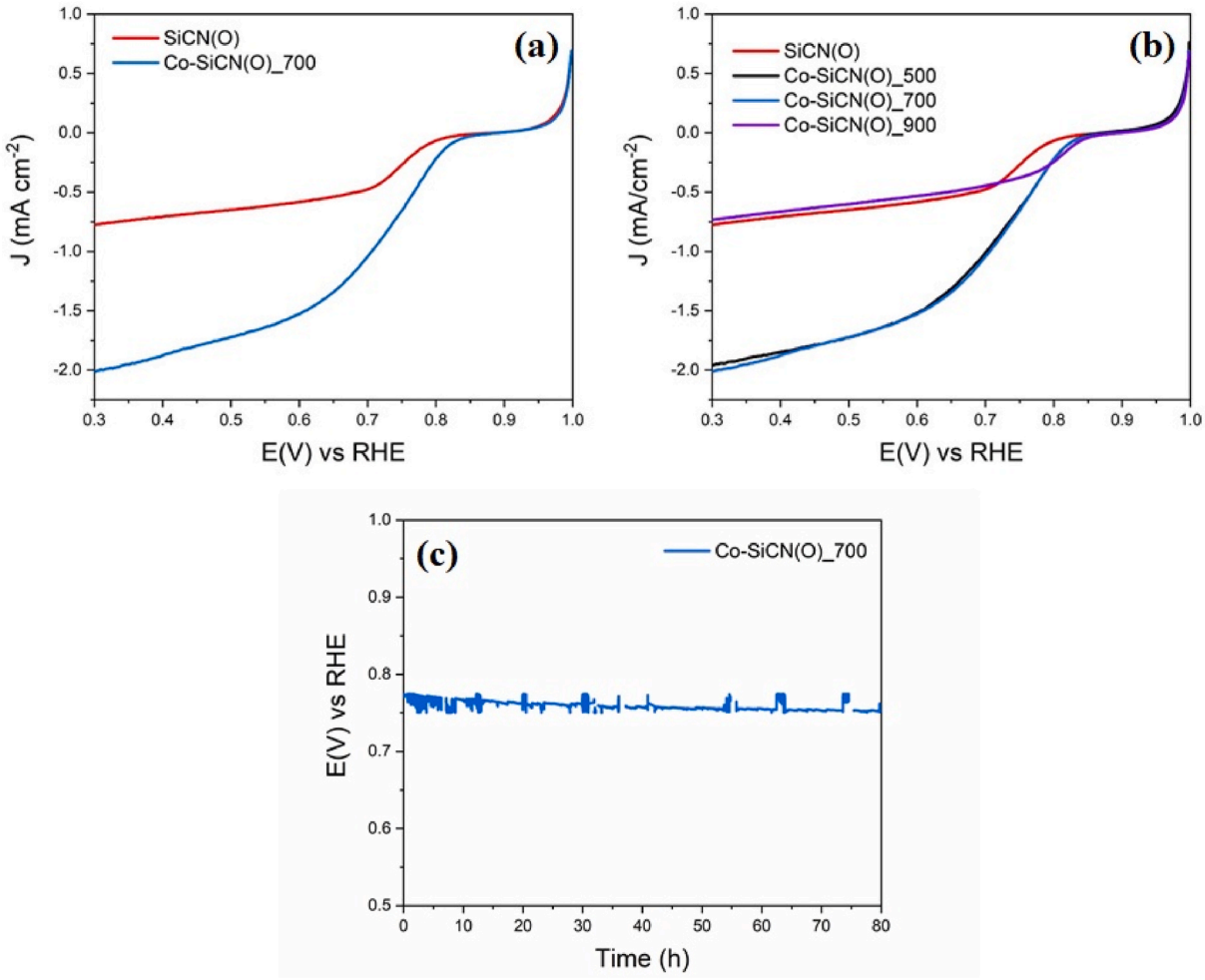

Fig. 8. Electrochemical activity of prepared catalysts towards ORR: (a) LSV of SiCN(O) and Co–SiCN(O)_700, (b) dependence on pyrolysis temperature and (c) Chronopotentiometric stability test performed at 10 mA cm^{-2} for 80 h.

demonstrating a potential drop of 24 mV in 3 days as shown in Fig. 8c, suggesting good stability with a performance degradation rate of 200 μV h^{-1}.

In the case of OER, Co–SiCN(O)_700 exhibited a potential of 1.67 V vs RHE at 10 mA cm^{-2} whereas SiCN showed poor OER activity (Fig. 9a). Interestingly, previous report on the OER activity of Co/PDC (Co loading - 0.02 mg cm^{-2}) based materials failed to reach the 10 mA cm^{-2} current density value in the measured potential range [28]. On similar note, Abhinaya et al. [30] reported a potential of 1.67 V vs. RHE for Co/SiOC catalysts. However, the catalyst loading used was almost twice the amount (0.5 mg cm^{-2}), highlighting the efficiency of Co–SiCN (O)_700 catalysts, probably in reason of the high dispersion degree of Co-base species in Co–SiCN(O)_700 sample. An additional strategy to diminish catalyst loading while enhancing catalytic activity involves the utilization of porous nanofibres as substrates. This strategy promotes faster kinetics and facilitates the mass and charge carriers [45]. The quantity of catalyst used plays a crucial role in influencing the current density. Given the relatively limited geometric area of the Glassy Carbon (GC) electrode at 0.196 cm^2, typical catalyst loadings on GC range from 0.1 to 0.5 mg cm^{-2}, with 0.2 mg cm^{-2} being the most prevalent [46]. In order to investigate the impact of Co loading on the OER apparent activity, two distinct loadings (0.01 and 0.1 mg cm^{-2}) were employed. The XRD analysis of Co–SiCN(O)_700 (0.1 mg cm^{-2}) revealed peaks at $2\theta = 44.3^{\circ}$, 51.6°, and 75.9°, corresponding to the (111), (200), and (220) planes of metallic cobalt, in line with the JCPDS card No. 15–0806 as shown in Fig. S5. As the loading increased, there was a noticeable increase in current density and a concurrent reduction in potential at 10 mA cm^{-2}, signifying enhanced OER apparent activity as illustrated in Fig. 9b. This could be attributed to increase in the number of catalytic sites. Moreover, the catalytic activity of Co–SiCN_700 (overpotential-360 mV) was far superior compared to other non-noble metal based electrocatalysts as shown in Table S1. An increase in the number of active sites correlated with enhanced mass transfer due to the porous nature of the fibres plays a major role in optimizing the electrocatalytic performance of the system [47]. This results in an increased Tafel slope, for Co–SiCN_700 (0.1 mg cm^{-2}) catalysts exhibiting a slope of 88 mV dec^{-1} in contrast to the Co–SiCN_700 (0.01 mg cm^{-2}) catalysts with a Tafel slope of 79 mV dec^{-1} (Fig. 9c). This trend persisted at higher current densities, indicating consistent shifts in Tafel slopes. The findings strongly imply that the Co loading plays a pivotal role in determining catalytic activity. A greater loading has an observable effect on current density, causing an upward shift. This could be attributed to the presence of a higher number of active sites in the reaction, underscoring the importance of metal loading in influencing overall catalytic performance. It is observed that the Co–SiCN_700 (0.1 mg cm^{-2}) exhibits a slightly higher Tafel slope value compared to the one with lower loading. It should be noted that as the amount is increased, the effective surface area decreases. The thicker layer of catalyst makes it difficult for electrons to move (due to enhanced resistance) between the catalyst and the substrate, indicating slower kinetics as implied from the Tafel's slope for Co–SiCN_700 (0.1 mg cm^{-2}).

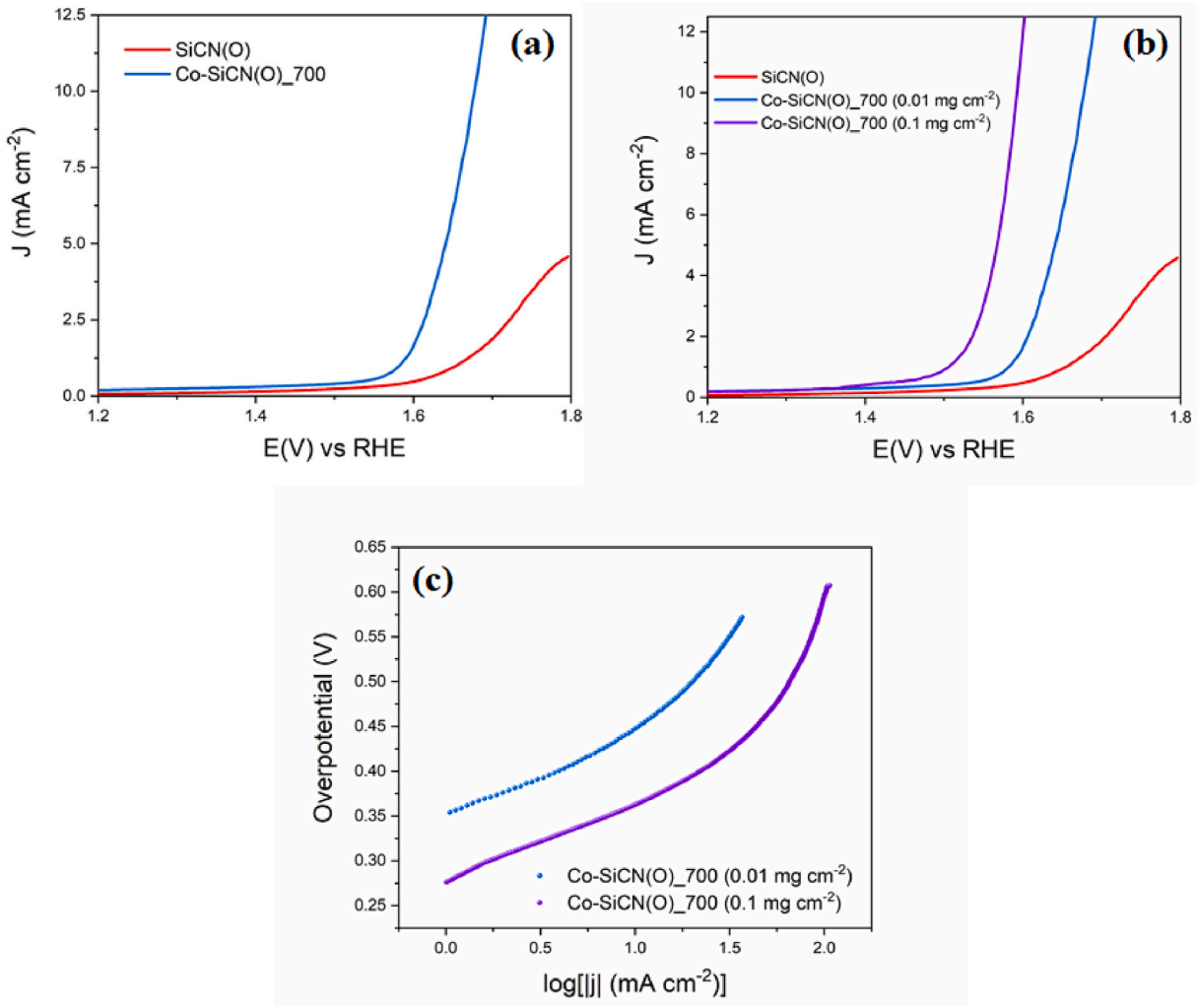

Fig. 9. Electrochemical activity of prepared catalysts towards OER: (a) OER performance of SiCN(O) and Co–SiCN(O)_700, (b) dependence on mass loading and (c) corresponding Tafel plots.

4. Conclusions

We successfully demonstrated a promising approach to generate and to immobilize Co nanoparticles on porous SiCN(O) ceramic fibre mats produced via electrospinning to act as a potential bifunctional electrocatalyst towards water splitting. The electrochemical evaluation revealed that the 4 wt% Co loaded SiCN(O) fibres exhibited significantly improved ORR/OER activity compared to conventional TM-based catalysts and other materials. The ultra-low loading of Co nanoparticles on the SiCN(O) fibre mats allowed for maximum utilization of the active surface sites, leading to efficient electron transfer and enhanced catalytic performance. Moreover, the desirable porosity of the SiCN(O) fibres facilitated the accessibility of reactants to the active sites, further enhancing the ORR/OER kinetics. The protective nitrogen doped carbon layers stabilize the Co nanocrystals and is expected to enhance the ORR activity. Additionally, the different binding modes of nitrogen present in the developed catalyst contributes to the enhanced ORR and OER kinetics. The findings from this study support the concept that ultra-low loading TM-support catalysts, particularly using Co on SiCN(O) fibres, can be a promising strategy to address the challenges associated with traditional ORR/OER catalysts. Notably, the economic viability of such catalysts can be improved by reducing the usage of expensive TMs while maintaining high electrochemical activity. The successful synthesis and evaluation of the Co loaded SiCN(O) fibres highlight the importance of tailoring the catalyst design to achieve superior electrochemical performance. Future research in this area should continue to explore other TMs and support materials to further optimize the ORR/OER activity while considering factors such as stability, durability, and scalability for practical applications. In summary, the investigation of ultra-low loading TM-support catalysts on porous SiCN(O) fibres via electrospinning has shown great promise for enhancing electrochemical activity in the context of ORR and OER activity. These findings contribute valuable insights to the development of efficient and cost-effective catalysts for renewable energy conversion and storage devices, ultimately advancing the field of sustainable energy technologies.

CRediT authorship contribution statement

Eranezhuth Wasan Awin: Writing – review & editing, Writing – original draft, Visualization, Investigation, Formal analysis, Data curation, Conceptualization. **Marwan Ben Miled:** Methodology, Formal analysis, Data curation. **Clément Comminges:** Methodology, Formal analysis, Data curation. **Aurélien Habrioux:** Writing – review & editing, Visualization, Supervision, Methodology, Investigation, Formal analysis. **Samuel Bernard:** Writing – review & editing, Supervision, Resources, Project administration, Funding acquisition, Conceptualization. **Stefan Schafföner:** Supervision, Project administration. **Günter Motz:** Writing – review & editing, Supervision, Resources, Project administration, Funding acquisition, Conceptualization.

Declaration of competing interest

The authors declare that they have no known competing financial interests or personal relationships that could have appeared to influence the work reported in this paper.

Acknowledgements

The authors would like to thank the Deutsche Forschungsgemeinschaft (DFG) and the Agence Nationale de la Recherche (ANR) for funding the work through the RECIFE project (DFG Project number 490841897 (MO851/22-1) and ANR-21-CE08-0036-01). SB and AH gratefully acknowledge the financial contribution from Nouvelle-Aquitaine region and IRCER (SYNERGY 2021 project N°AAPR2021A-2020–12007410; PhD of M. Ben Miled (MBM)). The authors greatly acknowledge the XPS facility at the Device Engineering KeyLab in the Bavarian Polymer Institute, University of Bayreuth.

Appendix A. Supplementary data

Supplementary data to this article can be found online at https://doi.org/10.1016/j.ijhydene.2024.09.206.

References

[1] Lin L, Zhu Q, Xu A. Noble-metal-free Fe-N/C catalyst for highly efficient oxygen reduction reaction under both alkaline and acidic conditions. J Am Chem Soc 2014;136:11027–33.
[2] Bezerra CWB, Zhang L, Lee K, Liu H, Marques EP, Wang H, et al. Review article A review of Fe-N/C and Co-N/C catalysts for the oxygen reduction reaction. Electrochim Acta 2008;53:4937–51.
[3] Online VA, Li S, Cong H, Wang P, Yu S. Flexible nitrogen-doped graphene/carbon nanotube/Co_3O_4 paper and its oxygen reduction activity. Nanoscale 2014;6:7534–41.
[4] Iqbal MZ, Kundu N, Sadhukhan D, Ghanty C. A facile route fabricated nickel-nitrogen-doped carbon nanoparticle based electrocatalysts for the oxygen evolution and hydrogen evolution reactions. ChemistrySelect 2023;8:1–9.
[5] Qiao M, Wang Y, Mamat X, Chen A, Zou G. Rational design of hierarchical, porous, Co-supported, N-doped carbon architectures as electrocatalyst for oxygen reduction. ChemSusChem 2020;13:741–8.
[6] Liu K, Zhong H, Meng F, Zhang X. Recent advances in metal-nitrogen-carbon catalysts for electrochemical water splitting. Mater Chem Front 2017;1:2155–73.
[7] Yoon KR, Hwang C, Kim S, Jung J, Chae JE, Kim J, et al. Hierarchically assembled cobalt oxynitride nanorods and N-doped carbon nano fibers for efficient bifunctional oxygen electrocatalysis with exceptional regenerative efficiency. ACS Nano 2021;15:11218–30.
[8] Sarapuu A, Samolberg L, Kreek K, Koel M, Matisen L, Tammeveski K. Cobalt-and iron-containing nitrogen-doped carbon aerogels as non-precious metal catalysts for electrochemical reduction of oxygen. J Electroanal Chem 2015;746:9–17.
[9] Lv L, Ye T, Gong L, Wang K, Su J, Li X, et al. Anchoring cobalt nanocrystals through the plane of graphene: highly integrated electrocatalyst for oxygen reduction reaction. Chem Mater 2015;27:544–9.
[10] Martı I, Rossmeisl J, Calle-vallejo F. Density functional studies of functionalized graphitic materials with late transition metals for oxygen reduction reactions. Phys Chem Chem Phys 2011;13:15639–43.
[11] Li R, Wang X, Dong Y, Pan X, Liu X, Zhao Z. Nitrogen-doped carbon nanotubes decorated with cobalt nanoparticles derived from zeolitic imidazolate framework-67 for highly efficient oxygen reduction reaction electrocatalysis. Carbon 2018;132:580–8.
[12] Sun T, Xu L, Li S, Chai W, Huang Y, Yan Y. Cobalt-nitrogen-doped ordered macro-/mesoporous carbon for highly efficient oxygen reduction reaction. Appl Catal B Environ 2016;193:1–8.
[13] Mo Q, Chen N, Deng M, Yang L, Gao Q. Metallic Cobalt@Nitrogen-doped carbon nanocomposites: carbon-shell regulation toward efficient bifunctional electrocatalysis. Appl. Mater. Interfaces 2017;9:37721–30.
[14] Wu B, Meng H, Morales DM, Zeng F, Zhu J, Wang B, et al. Nitrogen-rich carbonaceous materials for advanced oxygen electrocatalysis: synthesis, characterization, and activity of nitrogen sites. Adv Funct Mater 2022;32:2204137.
[15] Borup R, Meyers J, Pivovar B, Kim YS, Mukundan R, Garland N, et al. Scientific aspects of polymer electrolyte fuel cell durability and degradation. Chem Rev 2007;107:3904–51.
[16] Asghar H, Adeel M, Muhammad I, Iqbal A. Silicon-based carbonaceous electrocatalysts for oxygen reduction and evolution properties in alkaline conditions. SN Appl Sci 2019;1:1–10.
[17] Marı A. Si-CN for the oxygen reduction reaction in alkaline media, the effect of synthesis temperature. Int J Hydrogen Energy 2022;7:1–9.
[18] Mera G, Riedel R, Soraru GD. Polymer-derived ceramics: 40 Years of research and innovation in advanced ceramics. J Am Ceram Soc 2010;93:1805–37.
[19] Mera G, Gallei M, Bernard S, Ionescu E. Ceramic nanocomposites from tailor-made preceramic polymers. Nanomaterials 2015;5:468–540.
[20] Schumacher D, Wilhelm M. Porous SiOC monoliths with catalytic activity by in situ formation of Ni nanoparticles in solution-based freeze casting. J Am Ceram Soc 2020;103:2991–3001.
[21] Zaheer M, Hermannsdçrfer J, Kretschmer WP, Motz G. Robust heterogeneous nickel catalysts with tailored porosity for the selective hydrogenolysis of aryl ethers. ChemCatChem 2014;6:91–5.
[22] Gou Y, Tong X, Zhang Q, Wang B, Shi Q, Wang H, et al. The preparation and characterization of polymer-derived Fe/Si/C magnetoceramics. Ceram Int 2016;42:681–9.
[23] Polysilazane I, Viard A, Kurz H, Lale A, Heymann L, Weber B, et al. Superparamagnetic silicon carbonitride ceramic fibers through in situ generation of iron silicide nanoparticles during pyrolysis of an iron-modified polysilazane. ACS Appl Mater Interfaces 2021;13:8745–53.
[24] Cao Y, Yang X, An L. Electric conductivity and microstructure evolution of polymer-derived SiAlCO ceramics. Ceram Int 2016;42:4033–8.
[25] Niu J, Meng S, Jin H, Yi F, Li J, Zhang G, et al. Electrical conductivity change induced by porosity within polymer- derived SiCN ceramics. J Alloys Compd 2019;777:1010–6.
[26] Karoline R, Ferreira M, Miled B, Nishihora K, Christophe N, Carles P, et al. Nanoscale Advances Low temperature in situ immobilization of nanoscale fcc and hcp polymorphic nickel particles in polymer-derived Si-C-O-N(H) to promote electrocatalytic water oxidation in alkaline media. Nanoscale Adv 2023;5:701–10.
[27] Canuto T, Almeida D, Mooste M, Kibena-põldsepp E, Matisen L, Merisalu M, et al. Polymer-derived Co/Ni–SiOC(N) ceramic electrocatalysts for oxygen reduction reaction in fuel cells. Catal Sci Technol 2019;9:854–66.
[28] Moni P, Mooste M. One-dimensional polymer-derived ceramic nanowires with electrocatalytically active metallic silicide tips as cathode catalysts for Zn-air batteries. RSC Adv 2021;11:39707–17.
[29] Si M, Sic CC. Enhanced hydrogen evolution reaction catalyzed by carbon- rich $Mo_{4.8}Si_3C_{0.6}$/C/SiC nanocomposites via. A PDC approach. J Am Ceram Soc 2020;103:1385–95.
[30] Abinaya S, Moni P, Parthiban V, Sahu K. Metal silicide nanosphere decorated carbon-rich polymer-derived ceramics : bifunctional electrocatalysts towards oxygen and their application in anion exchange membrane fuel cells. Chemelectrochem 2019;6:3268–78.
[31] Hanniet Q, Boussmen M, Barés J, Huon V, Iatsunskyi I, Coy E, et al. Investigation of polymer-derived Si-(B)-C-N ceramic/reduced graphene oxide composite systems as active catalysts towards the hydrogen evolution reaction. Sci Rep 2020;10:1–15.
[32] Harms C, Murshed MM, Rezwan K. Metal-Containing ceramic composite with in situ grown carbon nanotube as a cathode catalyst for anion exchange membrane fuel cell and rechargeable zinc-air battery. Appl Energy Mater 2019;2:6079–86.
[33] Harms C, Adam M, Soliman KA, Wilhelm M. New electrocatalysts with pyrolyzed siloxane matrix. Electrocatal 2014;5:301–9.
[34] Rahaman MSA, Ismail AF, Mustafa A. A review of heat treatment on polyacrylonitrile fiber. Polym Degrad Stabil 2007;92:1421–32.
[35] Luo H, Lari L, Kim H, Hérou S, Tanase LC, Lazarov VK, et al. Structural evolution of carbon dots during low temperature pyrolysis. Nanoscale 2022;14:910–8.
[36] Mera G, Navrotsky A, Sen S, Kleebe H. Polymer-derived SiCN and SiOC ceramics – structure and energetics at the nanoscale. J Mater Chem A 2013;12:3826–36.
[37] Chem JM. Pyridinic N doped graphene: synthesis, electronic structure, and electrocatalytic property. J Mater Chem A 2011;21:8038–44.
[38] Chem JM, Zhao F, Huang Y. Grafting of polyhedral oligomeric silsesquioxanes on a carbon fiber surface : novel coupling agents for fiber/polymer matrix composites. J Mater Chem A 2011;21:3695–703.
[39] Brown AT, Lin J, Vizuet JP, Thomas MC, Balkus KJ. Graphene-like carbon from calcium hydroxide. ACS Omega 2021;6:31066–76.
[40] Wu J, Mehmood A, Zhang G, Wu S, Ali G, Kucernak A. Highly selective O_2 reduction to H_2O_2 catalyzed by cobalt nanoparticles supported on nitrogen-doped carbon in alkaline solution. ACS Catal 2021;11:5035–46.
[41] Zhao Y, Zhang J, Li K, Ao Z, Wang C, Liu H, et al. Electrospun cobalt embedded porous nitrogen doped carbon nano fibers as an efficient catalyst for water splitting. J Mater Chem A 2016;4:12818–24.
[42] Hu Y, Jensen JO, Zhang W, Cleemann LN, Xing W, Bjerrum NJ. Hollow spheres of iron carbide nanoparticles encased in graphitic layers as oxygen reduction. Catalysts Chem Int Ed 2014;53:3675–9.
[43] Bezerra CWB, Zhang L, Liu H, Lee K, Marques LB, Marques EP, et al. A review of heat-treatment effects on activity and stability of PEM fuel cell catalysts for oxygen reduction reaction. J Power Sources 2007;173:891–908.
[44] Ramavathu LN. Effect of pyrolysis temperature on cobalt phthalocyanine supported on carbon nanotubes for oxygen reduction reaction. Angew Chem Int Ed 2012;42:945–51.
[45] Shin S, Yoon Y, Park S, Shin MW. Fabrication of core-shell structured cobalt nanoparticle/carbon nanofiber as a bifunctional catalyst for the oxygen reduction/evolution reactions. J Alloys Compd 2023;939:168731.
[46] Jiang W, Lehnert W, Shviro M. The influence of loadings and substrates on the performance of nickel-based catalysts for the oxygen evolution reaction. Chemelectrochem 2023;10:1–9.
[47] Sung S, Yoo J. As featured in : energy & Environmental Science carbon as a support for oxygen evolution electrocatalysts. Environ Sci 2023;16:5019–28.